Journal of Academic Research Vol 30, Issu 1, 2026 "115-133"

Hydrogeochemical Characterizations and Groundwater Indicators in Al Batnan Area, Northeast Libya

Ahmed Mohammed*, Frag Adam, Ibrahim M. Abou El Leil

Geology Department, Faculty of Science, Tobruk University, Libya

ahmed.mohammed@tu.edu.ly

Article information

Key words

Groundwater. Hydrogeochemical. Water characterization. geochemical facies. Classification diagrams. stability indces.

Received **02 06 2026**, Accepted **22 06 2026,** Available online **22 06 2026**

Abstract

The supply of groundwater of acceptable quality has grown to be a major problem in many parts of the world, especially in locations near coasts that are impacted by seawater incursions, like the one under consideration. The main objective is to determine the groundwater's hydrogeochemical characterizations and their indicators, as well as its potential for scaling and corrosion. Samples of groundwater were taken from twelve pumping well locations. Major ions determination was the main focus of analyses carried out in accredited labs using standardised procedures. Gibbs diagrams, pipers trilinear, Durov, bar charts, radial plots, Chadha, and stiff diagrams are among the graphical techniques used. For water scaling and corrosion prediction, water stability indices such the Langelier saturation index (LSI), Ryznar stability index (RSI), Puckorius scaling index (PSI), and Aggressive index (AI) are utilized. The hydrochemistry results indicate that all of the water samples are alkaline and indicate that all groundwater samples are neutral to slightly alkaline. In the groundwater cationic dominance pattern, the predominant hydrochemical cations are $Na^+ > Ca2^+ > Mg^{2+} > K^+$; whereas the following is the order of the primary anions in groundwater: $Cl^- > SO42^- > HCO3- > CO3^-$. Based on Piper diagram all of the samples represents Na^+- K^+-Cl^- - $SO42^-$ ions revealed an acids $HCO3^-$ is the major anion. For Durov diagram, water samples are concentrated in the Cl- domain of the anionic triangle and $Ca2^+$-(Na^+-K^+) Ion exchange and the carbonate weathering zone are represented by the cationic triangle domain. The Chadha diagram showed that brackish water was mostly composed of Na^+ and Cl^- ions. Stiff diagrams demonstrate that whereas sodium, potassium, and calcium predominate in the cations, chlorine predominates in the anions with less bicarbonate. LSI, RSI, PSI, and AI are examples of water stability indicators that show scaling and corrosion potential.

I. Introduction

Groundwater is the most commonly used source of water supply worldwide. Depletion is an urgent worry, though, as rising demand has resulted in notable drops in groundwater levels. 97% of fresh water on Earth comes from groundwater, which is a significant water supply. According to [1], half of the water is set aside for drinking and the other half for watering. Inadequate water quality is the root cause of numerous illnesses and environmental issues. In order to satisfy human and other demands, water quality is just as crucial as its quantity and availability [2]. Groundwater with an excess of cations and anions is essential to millions of people [3]. An essential method for resolving many geochemical issues has been the character of groundwater in various

ahmed.mohammed@tu.edu.ly

aquifers over time and space ([4], [5], [6], [7]). Many different elements can dissolve in groundwater as a result of interactions with the atmosphere, surface environment, soil composition, and bedrock [8].Water quality is influenced by the total dissolved solids, which are determined by the solute load of the water. It is a very helpful indicator of the degree of pollution and contamination, soil or rock mass impacts, mode of formation within hydrological cycles, and geological evolution, among other things. Because groundwater has been in touch with rock for a longer period of time than shallow or young water, it often has substantially higher concentrations of most constituents.

Sea Water Intrusion

Sea water intrusion occurs when saline (salty) water from the ocean is drawn into a freshwater aquifer (groundwater source). Freshwater aquifers along the coast may be vulnerable to sea water intrusion due to physiographic and hydrogeologic conditions (Figure 1 at top). Sea water intrusion can affect a single well or multiple wells.

Pumping and changes in sea level and/or groundwater levels can cause sea water to migrate landward (Figure 1 at bottom). A large portion of a freshwater aquifer could be impacted if a single well is over-pumped or if multiple wells are pumping. Sea water intrusion may be permanent or take many years to reverse [(9,10)].

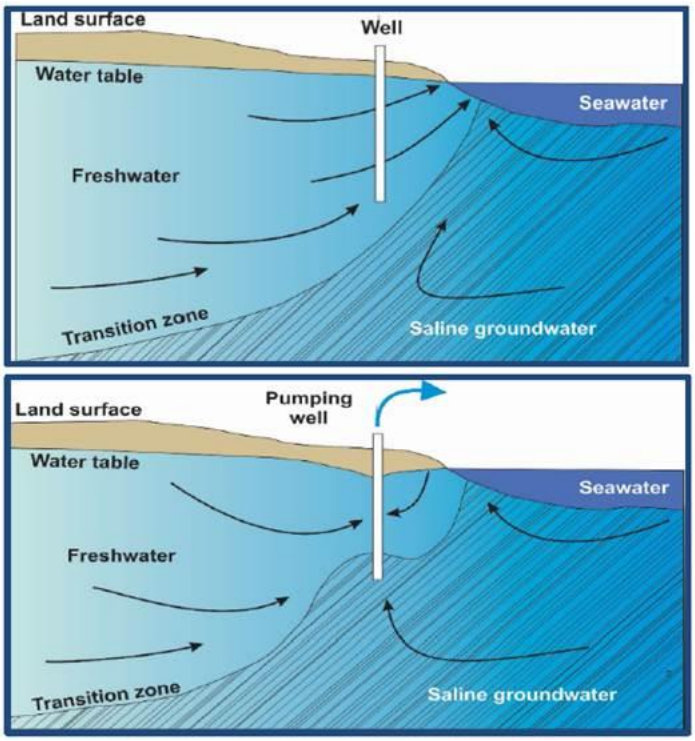

Fig. (1): Freshwater and saline groundwater has a natural equilibrium (A; top). Pumping or other disturbances can lead to landward migration of the interface between freshwater and saline groundwater.

The primary objectives of this study are to distinguish the impacts of seawater introusion into groundwater aquifers and to evaluate groundwater quality throughout calculation of their chemical indicators and the prediction of potential for scaling and corrosion processes in transmission pipelines or storage tanks.

Materials and Methods

The water samples were collected fro twelve pumping wells, designated GW1 through GW12 through autumn season. These wells are spread over several zones and encompassing Tobruk City as well as its suburbs, provided groundwater data. Using various analytical procedures, the samples are examined both chemically and physically.

The APHA [11] technique was followed in the chemical analysis of both cations and anions. The dissolved components can be conveniently separated into significant components, such as the dominating anions and cations. Sodium (Na^+), potassium (K^+), calcium (Ca^{2+}) and magnesium (Mg^{2+}) are dominant cations and bicarbonate (HCO_3^-), sulphate (SO_4^{2-}) and chloride (Cl^-) are dominant anions. The study shows how to use recognition techniques like (a) Chadha diagram, (b) Piper diagram, (c) Durov diagram, (d) Radial plot Gibbs diagram, and (f) Stiff diagram to identify the source contributions of important major ions in groundwater resources under different conditions by delineating the variations in chemical constituents.

Water stability indices were calculated for the investigated water. The potential for water scaling is indicated by the Langelier Saturation Index (LSI). The Ryznar Stability Index (RSI), Puckorius Scaling Index (PSI) and Aggressive Index (AI) can forecast scaling and corrosion in water samples with varying levels of hardness. Water samples from several wellheads were gathered for the current investigation, and geochemical parameters were examined. To find scaling potential in every sample, various indices were computed using geochemical data.
The Langelier saturation index (LSI) and the Ryznar stability index (RSI) are the two widely used techniques for determining the stability of water. LSI and RSI are intended to be prediction tools in relation to the calcium carbonates scale.

The study location of Al Batnan, which is represented by Tobruk City and its suburbs (Figure 2), was chosen. As shown on the map, groundwater data were gathered from several wells spread throughout this area. The wells can be described as located in different geologic setting and various rock formations such as limestones formation, dolomitic rock layers and calcareous shale and sometimes this rocks intercalated by shaly sandstones.

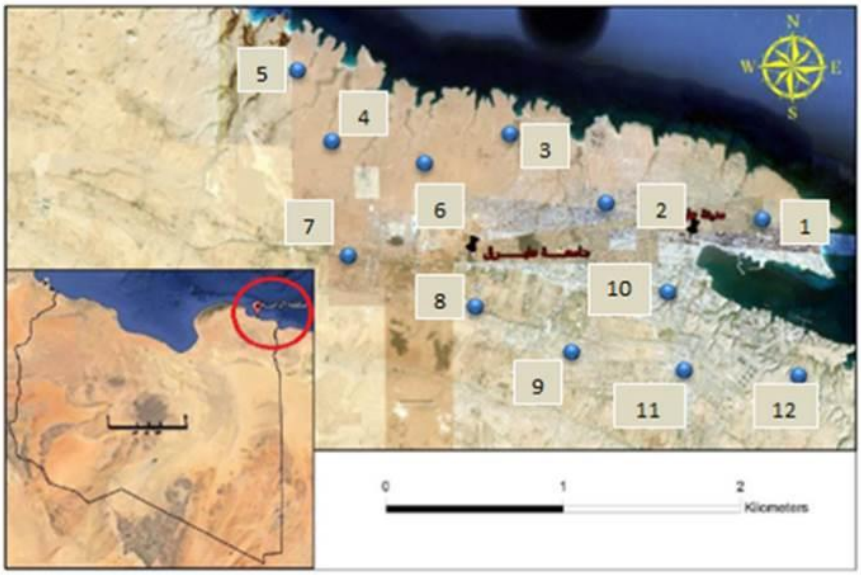

Fig. (2): Groundwater sample location map of the study area (Source: Google Earth).

Results and Discussion

Hydrochemistry of Groundwater

As seen in Tables 1 and 2, the measured physicochemical characteristics of the groundwater samples under study are statistically summarised and compared with the relevant acceptable requirements for drinking water standards established by the World Health Organisation [12].

Table 1: Physical properties and cations concentrations of groundwater samples.

Well No.	Well depth (m)	Physical properties			Cations (ppm)				
		pH	EC (μs/cm)	T (ºC)	TDS	Na^+	K^+	Ca^{++}	Mg^{++}
W1	97	7.2	810.20	22	4590	1922	38	920	64
W2	102	7.5	798.13	25	8640	1204	42	870	95
W3	86	6.9	992.85	24	12205	1690	44	760	89
W4	105	7.6	1016.20	23	14319	2995	51	902	97
W5	88	7.2	1013.90	26	6890	1102	62	640	72
W6	114	6.8	997.90	25	8875	1420	49	590	88
W7	110	6.4	680.32	26	3995	1802	58	450	67
W8	104	7.8	700.82	24	4805	1405	71	496	79
W9	117	7.3	910.20	23	14013	3102	62	1100	91
W10	121	6.6	1212.74	25	10290	2280	54	916	74
W11	109	6.9	1018.90	24	2669	1190	43	640	99
W12	104	7.1	814.87	25	9205	1520	39	790	81
Range	86-121	6.4-7.8	810.20-1212.74	22-26	3995-14319	1102-3102	38-71	450-1100	64-99
Average	104	7.10	913.92	24.42	8374.67	1802.67	51.08	756.17	83
WHO, 2017		8.5	1500	24.33	500	200	10	75	50

Table 2: Anions concentrations and other parameters of groundwater samples.

Well No.	Anions (ppm)				Alkalinity	Total Hardness (TH)
	Cl^-	$^-HCO_3$	$^-SO_4$	CO_3^{--}		
W1	2123	16	27	Tr	320	2560.60
W2	1504	12	32	Tr	415	2563.32
W3	2695	18	25	Tr	420	2263.96
W4	3095	14	19	Tr	399	2651.45
W5	2106	10	30	Tr	510	1444.90
W6	1922	11	27	Tr	760	1835.35
W7	2702	09	18	Tr	820	1399.36
W8	1905	12	14	Tr	612	1563.60
W9	3205	21	12	Tr	450	3121.17
W10	2485	18	22	Tr	620	2591.76
W11	2170	22	31	Tr	719	2005.47
W12	1990	19	24	Tr	388	2305.95
Range	1905-3205	09-22	12-32	--	320-820	1399.36-3121.17
Average	2325.17	15.17	23.47	--	536.08	2158.75
WHO, 2017	250	300	400	--	--	--

Physical Parameters

The pH and temperature ranges are 6.4 to 7.8 (average, 7.10) and 22°C to 26°C (average, 24.33°C), respectively (Table 1). The temperature is the average air temperature for the groundwater sampling period. The pH readings show that the groundwater under analysis has a neutral to slightly alkaline inclination. The calculated pH average value of 7.10 is indicative of free CO_2 availability in the analyzed groundwater as well as the soluble ions are fully in the form of HCO_3^- since pH and temperature have a significant impact on the dissolution of minerals in groundwater [13]. TDS ranges from 3995 to 14319 ppm (average, 8374.67) and EC ranges from 810.20 to 1212.74 µs/cm (average, 913.92 µs/cm), basically EC is proportionally with salinity and ion concentrations in water. Twenty percent of the samples surpass the WHO 2017 recommended EC and TDS limit (EC, 1500 µs/cm and TDS, 500 ppm). Water samples with TDS levels (TDS > 1000 ppm) are typically classified as brackish water groups [13]. Thses values are up normal contents if it is compared with that of fresh groundwater concentrations. Consequently, this is an indication of the affected by seawater intrusion. Also, human activity and geochemical processes have both affected the EC value ([14,15]).

Major Cations Chemistry

The pattern of cationic dominance is Na+ > Ca2+ > Mg2+ > K+ with relative abundance of 43.53%, 33.44%, 17.79% and 5.22% respectively. Sodium (Na+) is the most common cation, with a mean of 1802.67 ppm and a range of 1102 to 3102 ppm. The concentration of Na+ ion is also a good index for seawater intrusion into the groundwater aquifer. The samples surpass the WHO (2017) recommended tolerable limit of 200 pmm (Table 1). Na+ may be attributed to the influence of human and animal excrement as well as the weathering of rocks like halite and sodium plagioclase [14].

The prevalence of calcium-bearing minerals such limestone, dolomite, calcite, feldspar, etc. in the sedimentary formations containing groundwater is demonstrated by the fact that most sampling locations have higher Ca^{2+} values than Mg^{2+} [16]. Amphiboles, pyroxenes, and K-feldspars are examples of silicate minerals that contain calcium and produce Ca^{2+}. The content of calcium (Ca^{2+}) ranges from 4.50 to 1100 ppm, with an average of 756.17 ppm. The WHO (2017) limit of 75 ppm is exceeded in every sample.

The content of (Mg^{2+}) ranges from 64 to 99 ppm, with an average of 83 ppm. The samples are higher above the 50 ppm WHO drinking water standard standards. According to [17], the higher content of Mg^{2+} may result from the dissolution of Mg^{2+}-containing minerals as well as from the addition of Mg^{2+} to the groundwater from household and industrial waste. The average potassium (K^{+}) level is 51.08 ppm, with a range of 38 to 71 ppm. Every sample was higher above the WHO's allowed level of 10.0 ppm**.**

Major Anions Chemistry

The following is the order of the primary anions in groundwater: Cl^{-} > SO_4^{2-} > HCO_3^{-}> CO_3^{-} with their corresponding contribution of 98.28%, 1.12% and 0.65%. Cl^{-} concentration varies from 1905 to 3205 ppm, average 2325.17 ppm, is the most predominant anion in the groundwater, followed by followed by SO_4^{2-} (12 to 32 ppm, average, 23.47 ppm). On the other hand, Cl^{-} anion has a higher content in the grouwarwe samples similar with that concentration of Na^{+} cation. Both of them are representing the salinity content which has an average value 5992.92 ppm. This means that the water aquifer has been affected by seawater, because of the nture of groundwater can not be has this valus. Bicarbonate (HCO_3^{-}) is ranging from 09 to 22 ppm (average, 15.17 ppm), CO_3^{-} traces, . All samples are below the WHO (2017) permitted ranges (Table 2). HCO_3^{-} in subsurface water typically denotes fresh water [18] .The predominance of Ca^{2+} and HCO_3^{-} indicates that they originate from a similar source of minerals, such as the dissolution of carbonate minerals including limestone, calcite, dolomite, and chalk ([15], [19], [20]). Higher concentrations of HCO_3^{-} are found in areas with carbonate rocks, particularly limestones, according to spatial distribution samples.

Hydrochemical Facies

The three anions serve as the basis for the hydrochemical facies classification. (HCO3, Cl and SO4) and the cations (Na, K, Ca and Mg) calculated in meq/l, which occur in The primary chemical element is water. Piper and Durov's diagrams are among these classification basis.

The hardness of groundwater has a major impact on its appropriateness for domestic usage and drinking. The presence of alkaline earths causes the water's total hardness (TH). The following formula is utilised to calculate the TH = (2.497 Ca2+ + 4.115 Mg2+) in ppm [21]. According to the range of TH 1399.36 to 3121.17 ppm and the mean value 2158.75 ppm, the examined sample can be classified as hard water [22]. Figure 3 shows a comprehensive evaluation of groundwater quality based on TDS and TH [18], with all samples classified as hard-brackish groundwater. We would like to denote here that the differences between the nomencaluture and classification of groundwater under consideration is attributed to the different classification sources, each one of them has its specific classifications, but all of them are agreed that is hard water. However, the justifications of seawater intrusion can be expressed as following:

The studied area is located along sea coast.

1. The nature of groundwater is unacceptal as drinking fresh water.
2. The human activity for the intensive groundwater withdrwal and the unsuffient recharge of surface water lead to the intrusion of seawater in addition to other physiochemical processes.
3. The climatic changes and the lack of precipitation of rain fall through the last decade support that.
4. The nature of formations bearing water that can be characterized as porous media allowed for this phemomena.

5. These parameters are enough indices for seawater intrusion regardless to present any other indicators.

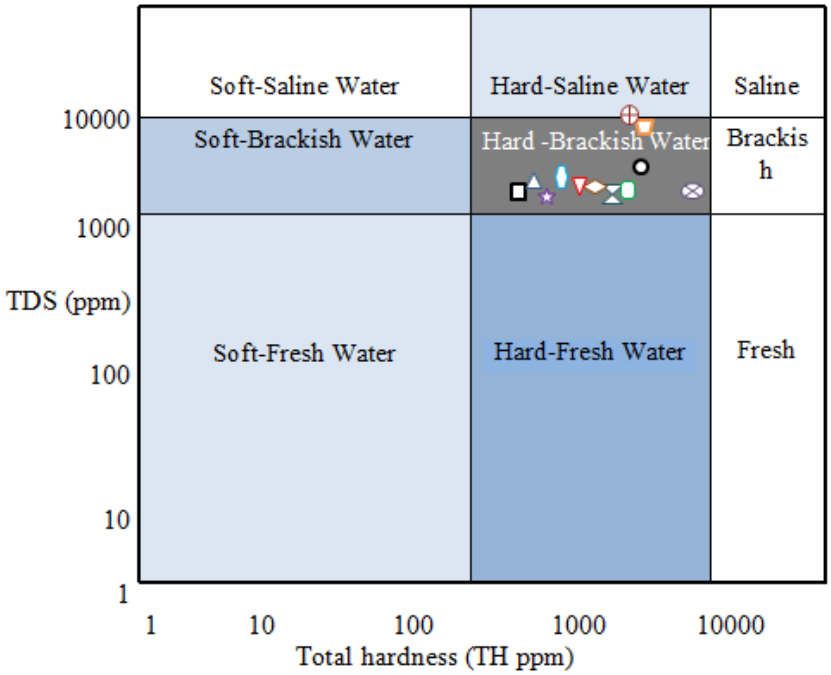

Fig. (3): Groundwater quality in the study area based on TDS and TH [18].

Based on the concentration of cations and anions, the water is categorised using hydrochemical facies ([23], [19]). As seen in Figures 4 and 5, the cationic and anionic data (meq/l) are expressed using the Piper trilinear diagram [24] .

Piper Trilinear Diagram

Traditional Piper plots ([25], [26]) can be used to plot the relative concentrations of the major ions on ternary diagrams. Based on the Piper diagram shown in Figure 4b, which is utilised to ascertain the chemical associations and groundwater dynamics over the research region. The groundwater was divided into four classes by this plot: i) Ca^{2+} - Mg^{2+}- Cl^{-} - SO_4^{2-}, ii)Na^{+}- K^{+} - Cl^{-} - $SO4^{2-}$ iii) Na^{+} - K^{+}- HCO3−, iv) Ca^{2+}- Mg^{2+}- HCO_3^{-} ([24, [27]). In the present study, all of the samples fall in field II which represents Na^{+}- K^{+}-Cl^{-} - SO_4^{2-} Weak acids and facies shows The main and dominant anion is Cl^{-}. In the present study, all samples fall within field II of the Piper diagram, representing Na–K–Cl–SO_4 water type. As illustrated in Figure 6, it can be categorised as saline water in addition to the sites D and G of sodium and chlorine kinds.

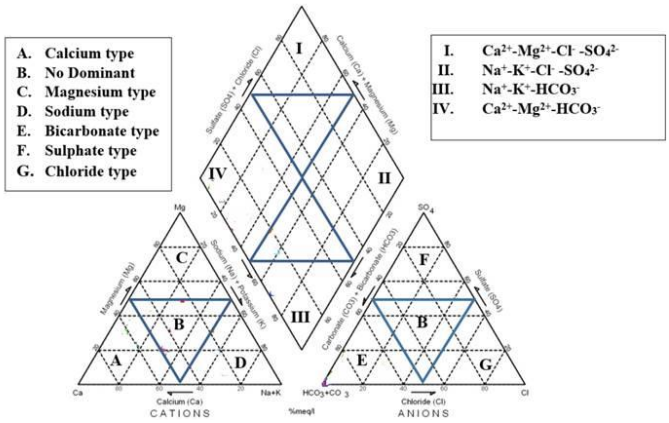

Fig. (4): Piper diagram for classifying groundwater

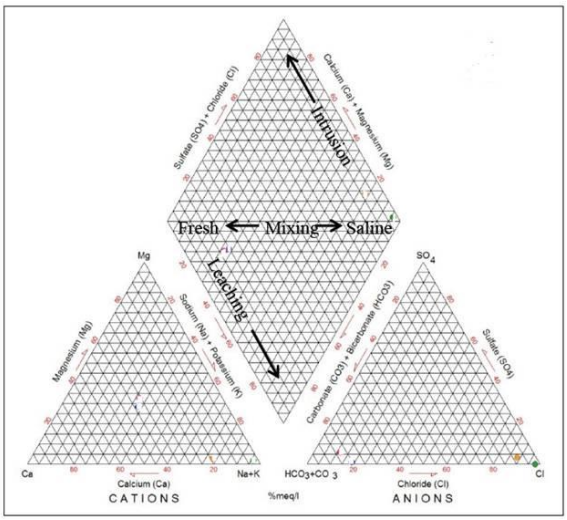

Fig. (5): Piper diagram for classifying groundwater.

Durov Diagram

In order to classify the different types of water, [28] created a different model that includes more details regarding hydrochemical facies. According to [29], it demonstrated a number of possible geochemical techniques for assessing and analysing groundwater quality. The Durov diagram shows the plot of the principal cations and anions.

On the Durov diagram, the main ion concentrations of water samples are also displayed. This figure is superior than the Piper diagram since it shows certain geochemical processes that may have an impact on the origin of water .

In the present Durov diagram, water samples are concentrated in the Cl- domain of the anionic triangle and Ca^{2+}-(Na^{+}-K^{+}) domain of the cationic triangle, representing carbonate weathering zone. On the other hand, in the cationic triangle, samples are together collected within the Ca^{2+}, intermediate and Na^{+}+ K^{+} water type domain. This ion distribution is consistent with the Ca^{2+}- Mg^{2+}- HCO_3^{-} and Na^{+} - K^{+} - HCO_3^{-} facies of Piper plot (Figure 6).

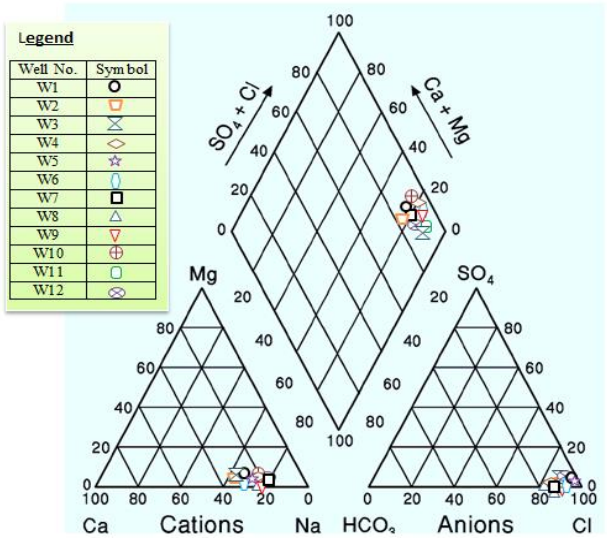

Fig. (6): Piper diagram representing hydrochemical facies of groundwater.

In the Durov diagram, majority of the samples are traced in the reverse cationic exchange field, where Ca^{2+}- Na^{+}- K^{+} is prevalent combined with dolomite and an important ion exchange is assumed when Na^{+} is dominant (Figure 6). Little of samples are in accordance with the features of modern infiltration of Ca^{2+}- Na^{+} - K^{+} type water [30].

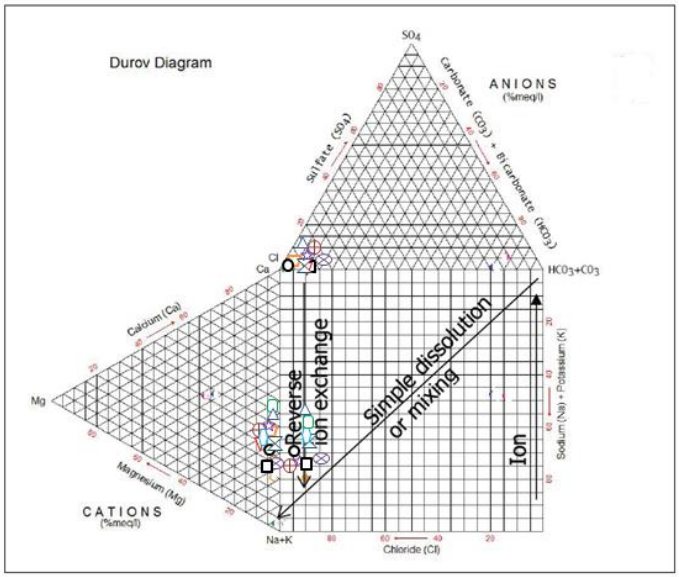

Fig. (7): Durov diagram of studied samples in the study area

Hydrogeochemical Evaluation

Gibbs plot

The mechanism and process governing groundwater chemistry are explained by the Gibbs plot [9] (Figure 8). The observed groundwater samples fall into the evaporation dominance domain. Additionally, groundwater is unaffected by precipitation or rock supremacy. The rock-water interaction zone is characterised by weathering of the rock, carbonate dissolution, precipitation, and ion exchange between water and clay-rich minerals [14]. The table shows that every sample under study had varying degrees of undersaturation with regard to all considered

minerals. The hydrogeological and geological conditions are responsible for the undersaturation state of all the minerals under study. Plotting allows for a general evaluation of the functional sources of dissolved ions. Na^{+}+ K^{+}/ Na^{+}+K^{+}+Ca^{2+} and Cl^{-}/Cl^{-}+HCO_3^{-} as a function of TDS [9] which indicate the chemical weathering of the rock forming minerals in the study area as shown in Figure 8.

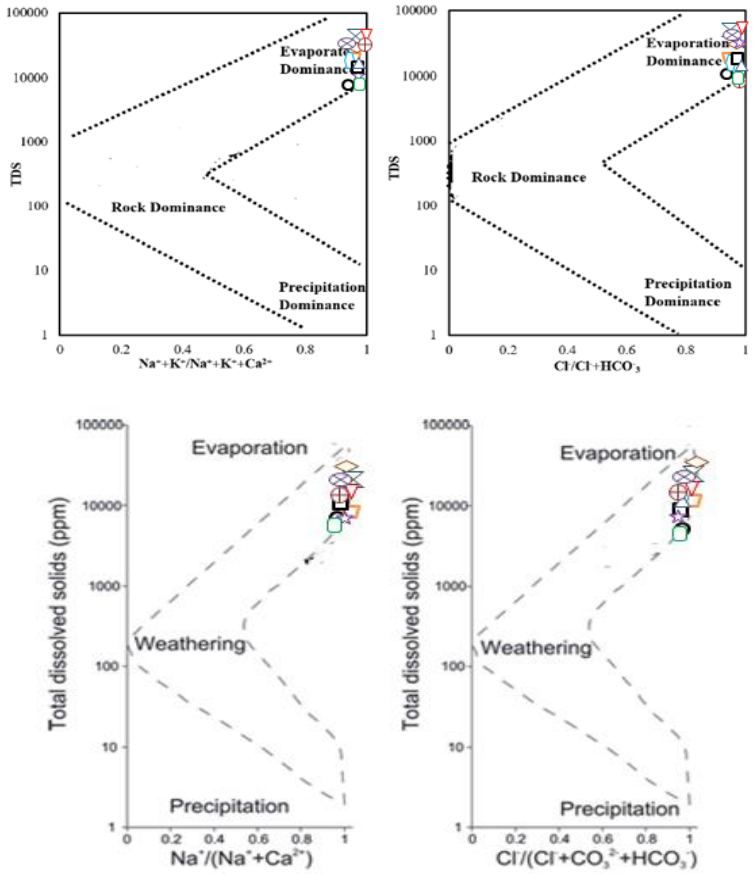

Fig. (8): Gibbs diagrams: TDS versus Na++ K+/ Na++K++Ca2+ and TDS versus Cl-/Cl-+HCO3- indicating the mechanisms controlling the groundwater chemistry

However, Figure 6 demonstrates that the water samples are situated in the upper third right of the graph, indicating the predominant evaporation process due to the high TDS and cationic or anionic ratio near 1.0.

Na-normalized Ca^{++} vs. Na^{+}-normalized Mg^{++} and HCO_3^{-} (Figure 9a, b) is constructed in accordance with [31] to assess the corresponding impact of the three primary weathering mechanisms (evaporite, carbonate, and silicate) that regulate the solute content in groundwater. These graphs show that most of the samples are in the evaporites dissolving field, which supports the earlier Gibbs classifications.

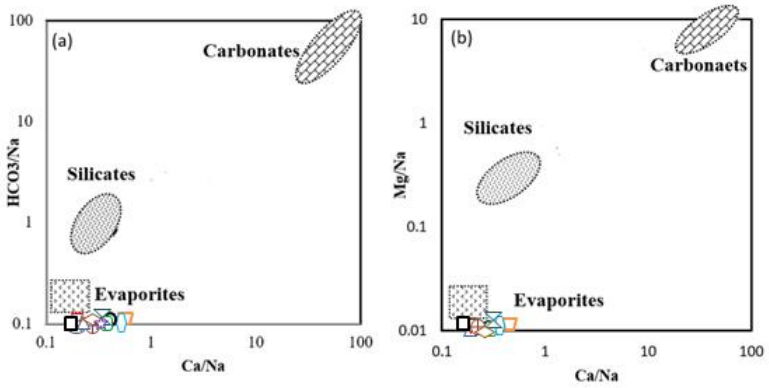

Fig. (9): Bivariate plots of a) Na-normalized HCO3 and Ca, b) Na-normalized Mg and Ca, presenting the trends of weathering. According to Mukherjee et al. (2012), the dotted areas represent the average groundwater compositions worldwide in terms of carbonate dissolution without mixing, silicate weathering, and evaporite dissolution.

Chadha Diagram

As seen in Figure 10, water samples that are dispersed around the lower left quadrant of the Chadha diagram are primarily composed of sodium and chloride ions and tend to be brackish.

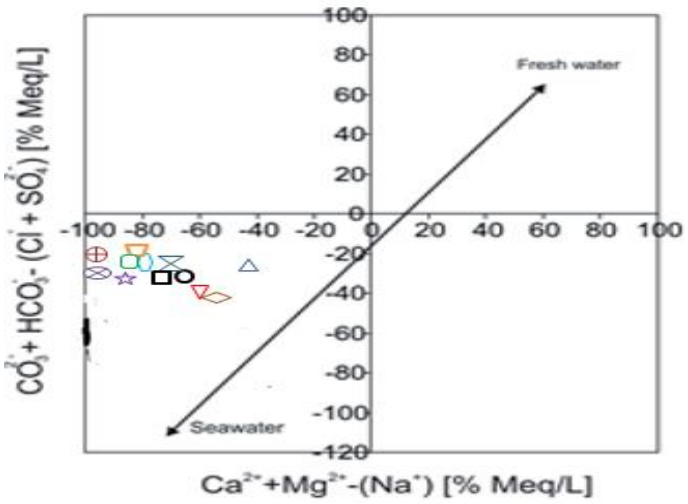

Fig. (10): Graphical representation of the Chadha diagram.

Radial Plot

The concentrations of the main ions in the groundwater in the wells under study were compared using radial plots. Both Cl- and Na+ The groundwater samples with the highest concentration of ions (Figure 11) are indicative of brackish water.

The radial plots show that Na+ and Cl− have the highest concentrations among the major ions, indicating that the groundwater is predominantly brackish (Figure 11).

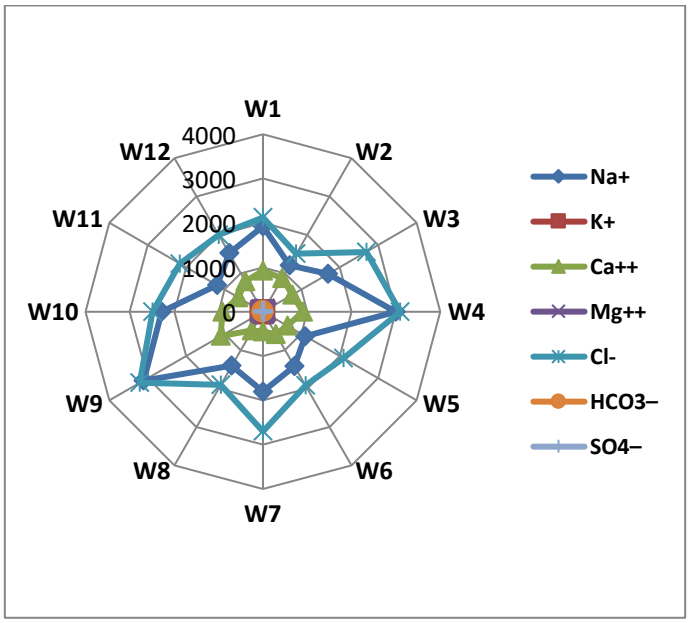

Fig. (11): Radial plot for the investigated groundwater.

Stiff Diagram

Plotting four cation concentrations to the left of the vertical zero axis and four anion concentrations to the right all values in milliequivalents per liter was suggested by [32]. Waters of comparable quality define a distinct shape from those of different quality, and the resultant points, when joined, produce an irregular polygonal pattern. The Stiff diagrams were plotted using the principal ion concentrations. Samples are identified by the shape they form.

Figure 12 from W1 to W12 illustrates that the cations are dominated by sodium, potassium, and calcium, while the anions are primarily dominated by chlorine with less bicarbonate.

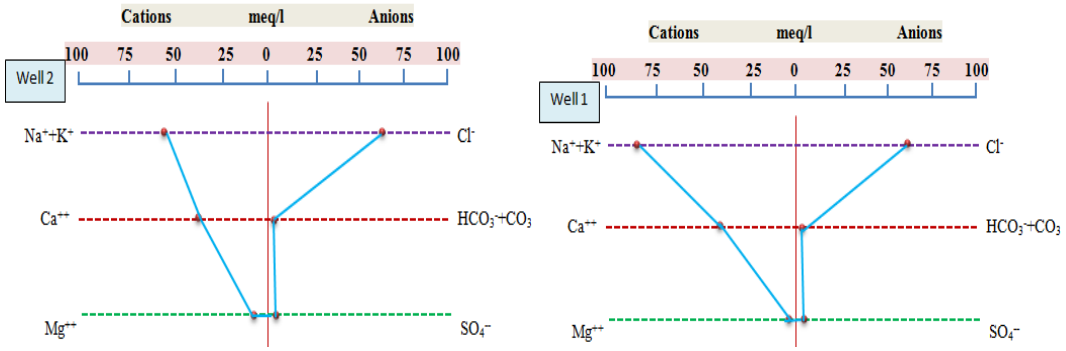

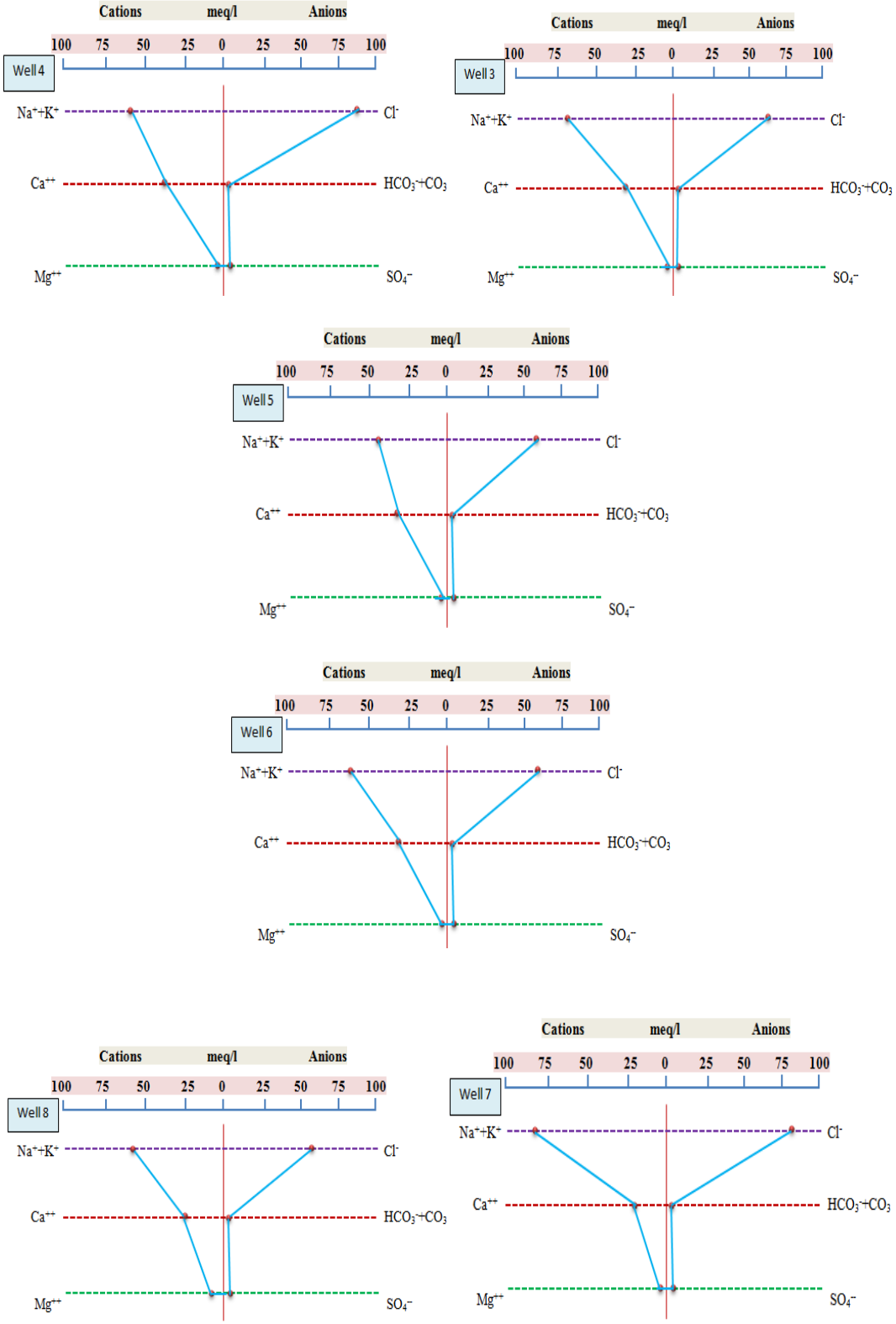
Cations
meq/l
Anions
100 75 50 25 0 25 50 75 100
Well 4
Na⁺+K⁺
Cl⁻
Ca⁺⁺
HCO₃⁻+CO₃
Mg⁺⁺
SO₄⁻
Well 3
Well 5
Well 6
Well 8
Well 7

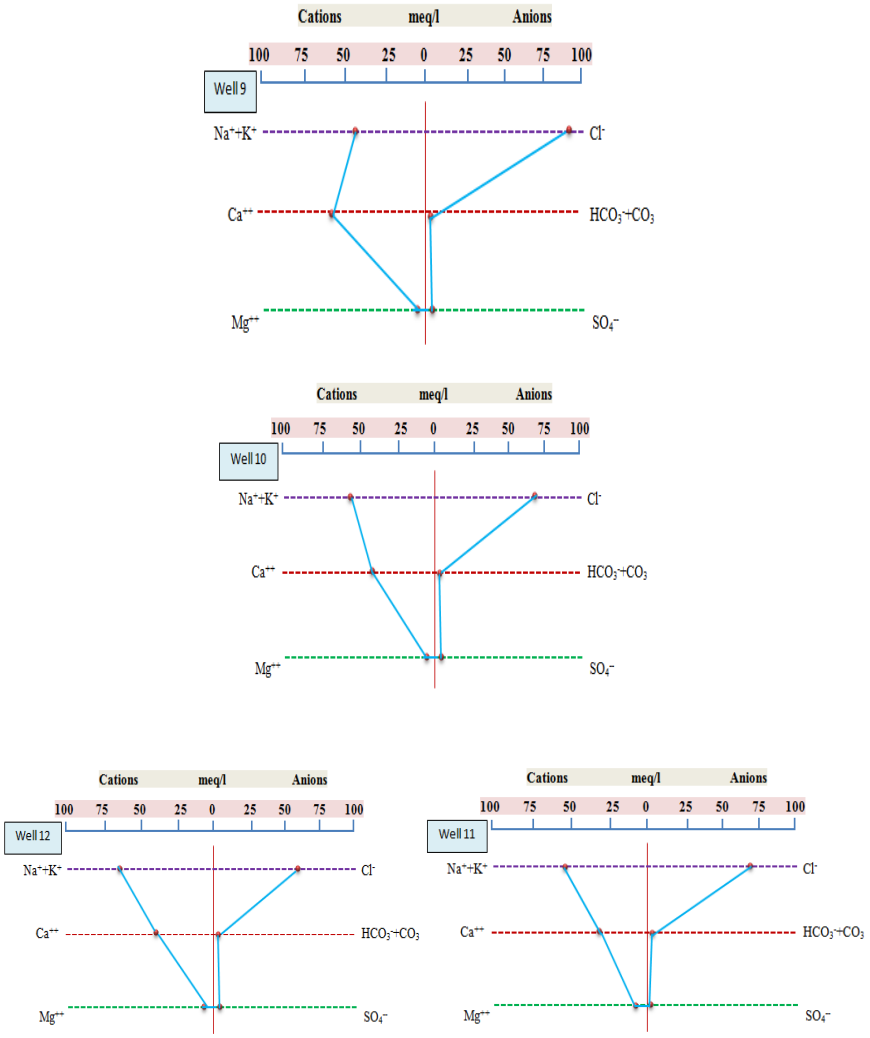

Fig. (12): Stiff diagrams for the investigated groundwater wells samples.

Prediction of Scaling and Corrosion

Using a various of chemical indicators, the corrosivity and scale formation are qualitatively predicted. The potential for water scaling is indicated by the Langelier Saturation Index (LSI). The Ryznar Stability Index (RSI) can forecast scaling and corrosion in water samples with varying levels of hardness. Water samples from several wellheads were gathered for the current investigation, and geochemical parameters were examined. To find scaling potential in every sample, various indices were computed using geochemical data .

Although numerous indices have been created, none have been able to measure or forecast the scaling or corrosive effects of water. They are only able to give an approximate indication [33]. The Langelier saturation index (LSI) and the Ryznar stability index (RSI) are the two widely used techniques for determining the stability of water. LSI and RSI are intended to be prediction tools in relation to the calcium carbonates scale. These methods cannot be used to estimate scales that contain silica, magnesium silicate, calcium phosphate, or calcium sulphate [34].The Aggressive Index (AI) and Puckorius Scaling Index (PSI) are additional instruments (Table 3).

Water Stability Indices

Despite the development of several indices, none have shown to be able to precisely measure and forecast the corrosive or scaling properties of water. They can only provide a likely indicator. Experience has demonstrated

that corrosion will typically be reduced if conditions promote the development of a protective calcium carbonate coating. The Langelier saturation index (LSI) and Ryznar stability index (RSI) are the most widely used techniques for determining water stability. Calcium phosphate, calcium sulphate, silica, and magnesium silicate scales cannot be estimated using LSI or RSI because they are intended to be prediction techniques for calcium carbonate scale [35].

The water stability indicators, which include LSI, RSI, PSI, and AI, have been computed for formation water while taking into account their potential for scaling and corrosion as well as their effects on petroleum facilities. Table 4 presents the results.

Table 3: Mathematical equations and classification of corrosiveness indices [34].

Index	Equation	Index value	Water condition
Langelier Saturation Index (LSI)	LSI = pH - pHs pHs = (9.3 +A + B) - (C + D) A = (Log (TDS)-1)/10 B = -13.2[Log (°C + 273)] + 34.55 C = Log (Ca++ + $CaCO_3$) D = Log (Alkalinity as $CaCO_3$)	LSI < 0	Corrosion occurs
		LSI = 0	Neutral
		LSI > 0	Scaling occurs
Ryznar Stability Index (RSI)	RSI= 2pHs -pH	RSI < 5.5	High scale forming
		5.5 < RSI < 6.2	Low scale-forming
		6.2 ≤ RSI ≤ 6.8	Neutral
		6.8 < RSI < 8.5	Low corrosive
		RSI ≥8.5	High corrosive
Puckorius Scaling Index (PSI)	PSI = 2pHs - pHeq pHeq = 1.465log (Alkalinity) + 4.54	PSI > 7	Corrosion occurs
		PSI < 6	Scaling occurs
Aggressive Index (AI)	AI = pH + log [(Ca^{++}) (Alkalinity)]	AI < 10	Corrosion occurs
		10 ≤ AI ≤ 12	Moderately corrosive
		AI > 12	Scaling occurs

pH = Actual, pHs = Saturated pH, pHeq = Equivalent pH

Table 4: Water stability indices.

Water stability indices				
Well No.	LSI	RSI	PSI	AI
W1	1.27	4.66	3.65	12.67
W2	1.75	4.00	3.12	13.06
W3	1.07	4.76	3.28	12.40
W4	1.76	7.60	3.38	13.16
W5	1.52	4.16	2.85	12.89
W6	1.22	4.38	2.42	12.45
W7	1.05	4.30	1.89	11.97
W8	2.14	3.52	2.70	13.41
W9	1.60	4.12	2.99	12.99
W10	1.09	4.42	2.39	12.35
W11	1.44	4.02	2.19	12.56
W12	1.27	4.56	3.33	12.59
Scaling and corrosive prediction	LSI > 0 Scaling occurs	RSI < 5.5 High scale forming	PSI < 6 Scaling occurs	AI > 12 Moderately corrosive and scaling occurs

Table 4 presents the scaling and corrosin predictions based on a correlation between the actual results and the propsal values of the earlier writers. Both LSI, PSI, and AI are showing scaling and corrosion processes, according to the correlations that were found. In general, it can be said that this water will have a detrimental effect on metallic structures and pipe lines .

However, as seen in Figure 13, these water stability index data are graphically produced to illustrate the variance between the various indices throughout the twelve groundwater wells. They clearly differ from well to well, and this is unquestionably due to the physiochemical characterisation of every well. this of course attributed to some factors such as well depth to reach groundwater table and the essentialy reason is the variation of water bearing formations that penetrated by this wells, e.g. limestone beds, dolomitic rocks and shaley calcareous rocks.

Conclusion

The following conclusions can be made in light of the earlier study:

1. The physiochemical analysis provides a straightforward and efficient means of displaying hydrogeochemical data and related information.

2.The cationic dominance pattern is Na+ > Ca2+ > Mg2+ > K+; while the principle anions in groundwater are in the following order Cl− > SO42− > HCO3−> CO3−.

3. Gibbs diagrams, pipers trilinear, Durov, bar charts, radial plots, Chadha, and stiff diagrams are among the graphical approaches used. Graphical methods are visible and simple to understand.

4.Based on Piper diagram all of the samples represents Na+- K+-Cl− - SO42− facies reveals and weak acids HCO3− is the major anion.

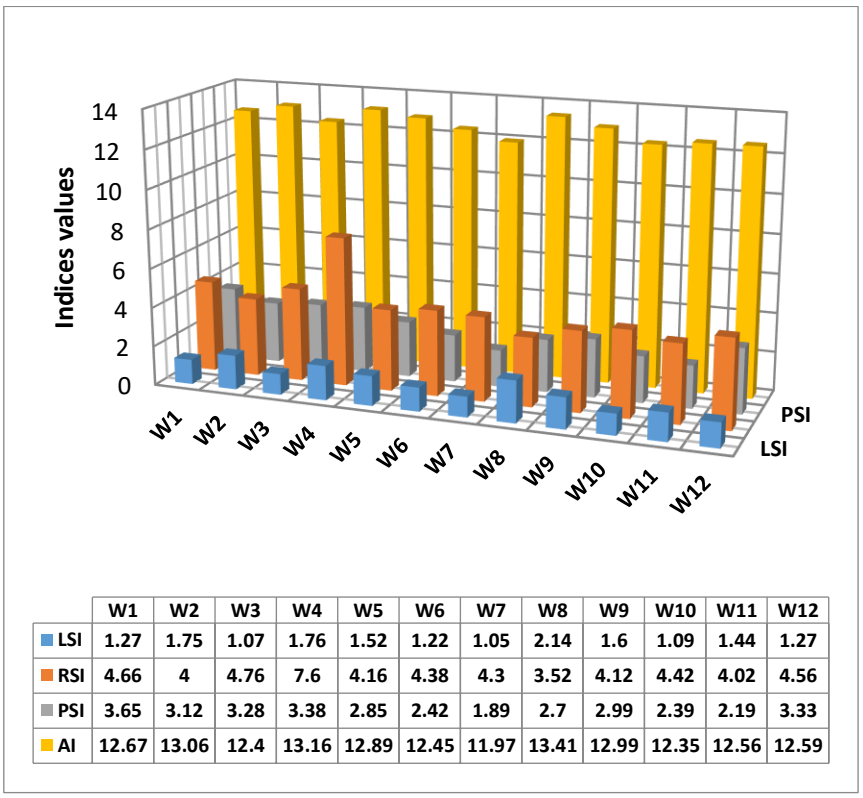

	W1	W2	W3	W4	W5	W6	W7	W8	W9	W10	W11	W12
LSI	1.27	1.75	1.07	1.76	1.52	1.22	1.05	2.14	1.6	1.09	1.44	1.27
RSI	4.66	4	4.76	7.6	4.16	4.38	4.3	3.52	4.12	4.42	4.02	4.56
PSI	3.65	3.12	3.28	3.38	2.85	2.42	1.89	2.7	2.99	2.39	2.19	3.33
AI	12.67	13.06	12.4	13.16	12.89	12.45	11.97	13.41	12.99	12.35	12.56	12.59

Fig. (13):Graphical plot of water stability indces

5.Water samples are concentrated in the carbonate weathering zone represented by the Cl-domain of the anionic triangle and the Ca2+-(Na+-K+) domain of the cationic triangle for the Durov diagram.
6. Additionally, the bulk of the samples in the Durov diagram are traced in the reverse cationic exchange field, where Na+ is believed to be the main ion exchange and Ca2+-Na+-K+ is common when paired with dolomite.

7.The Gibbs plot indicates that the water samples, which are the primary process of evaporation, are situated in the upper third right of the graph.

8.Water samples are dispersed over the lower left quadrant of the Chadha diagram, with a tendency towards brackish water and mostly sodium and chloride ions.

9.Stiff diagrams reveal that the cations are dominated by sodium, potassium, and calcium, whereas the anions are mostly dominated by chlorine with less bicarbonate.

10.The water stability indicators, which include LSI, RSI, PSI, and AI AI, show the possibility of corrosion and scaling.

Recommendations

Based on the previous findings of this study the following recommendations can be suggested:

1- The area under consideration required additional geological study because of it is characterized by complex geological structurs particularly along the coastal line, consequently may be affected to the seawater intrusion into groundwater aquifers.
2- Stratigraphic and correlation study must be done to assess the formation bearing water all over the area.
3- The study should be carried out through the four seasons of a year.
4- Distinguis the variation of groundwater table all over the area.

References

[1] V. Vadiati, J. Adamowski, and A. Beynaghi, “A brief overview of trends in groundwater research: Progress towards sustainability?,” Journal of Environmental Management, vol. 223, pp. 849–851, 2018, doi: 10.1016/j.jenvman.2018.06.086.
[2] A. Jakeman, O. Barreteau, R. J. Hunt, J. D. Rinaudo, and A. Ross, Integrated Groundwater Management: Concepts, Approaches and Challenges. Berlin, Germany: Springer, 2016, ISBN: 978-3-319-23576-9.
[3] S. T. Ramesh, R. Gandhimathi, P. V. Nidheesh, and M. Taywade, “Batch and column operations for the removal of fluoride from aqueous solution using bottom ash,” Environmental Research, Engineering and Management, vol. 60, no. 2, pp. 12–20, 2012.
[4] I. I. Chebotarev, “Metamorphism of natural waters in the crust of weathering,” Geochimica et Cosmochimica Acta, vol. 8, pp. 22–28, 1955, doi: 10.1016/0016-7037(55)90015-6.
[5] J. D. Hem, Study and Interpretation of the Chemical Characteristics of Natural Water. U.S. Geological Survey Water Supply Paper, 1959, pp. 269–271.
[6] W. Back and B. Hanshaw, “Chemical geohydrology,” in Advances in Hydroscience. New York, NY, USA: Academic Press, 1965, pp. 49–109.
[7] R. J. Gibbs, “Mechanisms controlling world water chemistry,” Science, vol. 170, no. 3962, pp. 1088–1090, 1970, doi: 10.1126/science.170.3962.1088.
[8] V. Subramanian, Water: Quantity and Quality Perspective in South Asia. Surrey, U.K.: Kingston International Publishers, 2000.
[9] J. Ayari, H. Ouelhazi, A. Charef, and A. Barhoumi, “Delineation of seawater intrusion and groundwater quality assessment in coastal aquifers: The Korba coastal aquifer (Northeast Tunisia),” Marine Pollution Bulletin, vol. 188, Art. no. 114643, 2023.

[10] M. D. Fidelibus, G. Balacco, M. R. Alfio, et al., "A chloride threshold to identify the onset of seawater/saltwater intrusion and a novel categorization of groundwater in coastal aquifers," Journal of Hydrology, vol. 653, Art. no. 132775, 2025, doi: 10.1016/j.jhydrol.2025.132775.
[11] APHA, AWWA, and WPCF, Standard Methods for the Examination of Water and Wastewater, 20th ed. Washington, DC, USA: American Public Health Association, 1998.
[12] World Health Organization, Guidelines for Drinking-Water Quality: First Addendum to the Fourth Edition. Geneva, Switzerland: WHO, 2017.
[13] R. A. Freeze and J. A. Cherry, Groundwater. Englewood Cliffs, NJ, USA: Prentice-Hall, 1979.
[14] K. N. Rao and P. S. Latha, "Groundwater quality assessment using water quality index with a special focus on vulnerable tribal region of Eastern Ghats hard rock terrain, Southern India," Arabian Journal of Geosciences, vol. 12, pp. 1–16, 2019.
[15] S. Selvam, S. Venkatramanan, S. Y. Chung, and C. Singaraja, "Identification of groundwater contamination sources in Dindugal district of Tamil Nadu, India using GIS and multivariate statistical analyses," Arabian Journal of Geosciences, vol. 9, 2016.
[16] K. K. Yadav, N. Gupta, V. Kumar, P. Choudhary, and S. A. Khan, "GIS-based evaluation of groundwater geochemistry and statistical determination of the fate of contaminants in shallow aquifers from different functional areas of Agra city, India: Levels and spatial distributions," RSC Advances, vol. 8, no. 29, pp. 15876–15889, 2018, doi: 10.1039/C8RA00577J.
[17] M. Bodrud-Doza, M. A. H. Bhuiyan, S. D. U. Islam, M. S. Rahman, M. M. Haque, K. J. Fatema, and M. A. Rahman, "Hydrogeochemical investigation of groundwater in Dhaka City of Bangladesh using GIS and multivariate statistical techniques," Groundwater for Sustainable Development, vol. 8, pp. 226–244, 2019, doi: 10.1016/j.gsd.2018.11.008.
[18] P. S. Kumar, "Evolution of groundwater chemistry in and around Vaniyambadi industrial area: Differentiating the natural and anthropogenic sources of contamination," Chemie der Erde – Geochemistry, vol. 74, no. 4, pp. 641–651, 2014, doi: 10.1016/j.chemer.2014.02.002.
[19] N. Ahmed, M. Bodrud-Doza, S. M. D. U. Islam, et al., "Hydrogeochemical evaluation and statistical analysis of groundwater of Sylhet, north-eastern Bangladesh," Acta Geochimica, vol. 38, pp. 440–455, 2019, doi: 10.1007/s11631-018-0303-6.
[20] R. Barzegar, A. Asghari Moghaddam, S. Soltani, et al., "Heavy metal(loid)s in the groundwater of Shabestar area (NW Iran): Source identification and health risk assessment," Exposure and Health, vol. 11, pp. 251–265, 2019, doi: 10.1007/s12403-017-0267-5.
[21] J. T. Todd, L. S. Mark, R. E. Shaw, and J. B. Pittenger, "The perception of human growth," Scientific American, vol. 242, no. 2, pp. 132–145, 1980.
[22] C. N. Sawyer and P. L. McCarty, Chemistry for Sanitary Engineers. New York, NY, USA: McGraw-Hill, 1967.
[23] S. D. U. Islam, R. K. Majumder, M. J. Uddin, M. I. Khalil, and A. M. Ferdous, "Hydrochemical characteristics and quality assessment of groundwater in Patuakhali district, southern coastal region of Bangladesh," Exposure and Health, vol. 9, pp. 43–60, 2017, doi: 10.1007/s12403-016-0221-y.
[24] A. M. Piper, "A graphic procedure in the geochemical interpretation of water analyses," Eos, Transactions American Geophysical Union, vol. 25, no. 6, pp. 914–928, 1944, doi: 10.1029/TR025i006p00914.
[25] M. Irani, M. Salimi, F. G. Talouki, et al., "Assessing the impacts of climate change on the vulnerability of coastal aquifers to seawater intrusion," Discover Civil Engineering, vol. 1, p. 109, 2024.
[26] B. Winid and M. Mavuta, "Assessment of groundwater vulnerability to seawater intrusion in the Polish Baltic coastal region," Water, vol. 17, no. 3, p. 366, 2025.

[27] P. Li, X. Li, X. Meng, M. Li, and Y. Zhang, "Appraising groundwater quality and health risks from contamination in a semiarid region of northwest China," Exposure and Health, vol. 8, pp. 361–379, 2016, doi: 10.1007/s12403-016-0205-y.

[28] S. A. Durov, "Natural waters and graphic representation of their composition," Doklady Akademii Nauk SSSR, vol. 59, no. 3, pp. 87–90, 1948.

[29] O. S. Onwuka and O. V. Omonona, "Hydrogeochemical characteristics of coastal aquifers from Port Harcourt, southern Nigeria," Environmental Earth Sciences, vol. 76, pp. 1–16, 2017, doi: 10.1007/s12665-017-6933-x.

[30] J. Makni, S. Bouri, and H. Ben Dhia, "Hydrochemistry and geothermometry of thermal groundwater of southeastern Tunisia (Gabes region)," Arabian Journal of Geosciences, vol. 6, pp. 2673–2683, 2013, doi: 10.1007/s12517-011-0510-5.

[31] A. Mukherjee and A. E. Fryar, "Deeper groundwater chemistry and geochemical modeling of the arsenic affected western Bengal basin, West Bengal, India," Applied Geochemistry, vol. 23, no. 4, pp. 863–894.

[32] H. A. Stiff Jr., "The interpretation of chemical water analysis by means of patterns," Transactions of the AIME, vol. 192, pp. 376–379, 1951.

[33] J. R. Rossum and D. T. Merrill, "An evaluation of the calcium carbonate saturation indexes," Journal of the American Water Works Association, vol. 75, pp. 95–100, 1983.

[34] A. S. Alsaqqar, B. H. Khudair, and S. K. Ali, "Evaluating water stability indices from water treatment plants in Baghdad City," Journal of Water Resource and Protection, vol. 6, pp. 1344–1351, 2014.

[35] M. Benaafi, S. I. Abba, and I. H. Aljundi, "Effects of seawater intrusion on the groundwater quality of multi-layered aquifers in Eastern Saudi Arabia," Molecules, vol. 28, no. 7, Art. no. 3173, 2023.

الخصائص الهيدروجيوكيميائية وجودة المياه الجوفية في منطقة البطنان، شمال شرق ليبيا

أحمد محمد*،، فرج آدم، إبراهيم م. أبو الليل

قسم الجيولوجيا، كلية العلوم، جامعة طبرق، ليبيا
ahmed.mohammed@tu.edu.ly

استلمت الورقة بتاريخ 2026/06/02، وقبلت بتاريخ 2026/06/22، ونشرت بتاريخ 2026/06/22

الكلمات المفتاحية: :
المياه الجوفية.
الهيدروجيولوجيا الكيميائية.
خصائص المياه.
الأنماط الجيوكيميائية.
مخططات التصنيف.
مؤشرات الاستقرار.

الملخص

أصبح توافر المياه الجوفية ذات الجودة المقبولة مشكلة كبيرة في العديد من مناطق العالم، خاصة في المواقع القريبة من السواحل التي تتأثر بتسرب مياه البحر، مثل الموقع الذي يتم النظر فيه. تزداد حدة هذه المشكلة بسبب الطقس القاسي والتلوث، مما يجعل إمدادات المياه الجوفية أكثر عرضة للعديد من أنواع التلوث. الهدف الرئيسي من هذه الدراسة هو تحديد الوجوه الجيوكيميائية للمياه الجوفية، بالإضافة إلى إمكانياتها للتكلس والتآكل. تهدف الدراسة أيضًا إلى تحديد مصادر التمعدن التي تؤثر على هذه المجاري المائية. تم أخذ عينات من المياه الجوفية من اثني عشر موقعًا لمضخات الآبار. كان تحديد الأيونات الرئيسية هو التركيز الرئيسي للتحليلات التي أجريت في مختبرات معتمدة باستخدام إجراءات موحدة. تشمل التقنيات الرسومية المستخدمة مخططات جيبس، ومخططات بايبر الثلاثية، ومخططات دوروف، والمخططات الشريطية، والمخططات الشعاعية، ومخططات تشادا، ومخططات ستيف. لتوقع التكلس والتآكل في المياه، يتم استخدام مؤشرات استقرار المياه مثل مؤشر تشبع لانجيلييه (**LSI**)، مؤشر استقرار ريزنار (**RSI**)، مؤشر تكلس باكورياس (**PSI**)، ومؤشر العدوانية (**AI**). تشير نتائج الكيمياء المائية إلى أن جميع عينات المياه قلوية. في نمط الهيمنة الكاتيونية للمياه الجوفية، فإن الوجهة الهيدروكيميائية السائدة هي **Na+ > Ca2+ > Mg2+ > K+**؛ بينما يكون ترتيب الأنيونات الرئيسية في المياه الجوفية كما يلي: **Cl− > SO42− > HCO3− > CO3**−. استنادًا إلى مخطط بايبر، تمثل جميع العينات وجهات نظر **Na+- K+- SO42 - Cl−**، وتظهر الأحماض الضعيفة **HCO3**− كالأيون الرئيسي. بالنسبة لمخطط دوروف، تتركز عينات المياه في مجال **Cl-** من مثلث الأيونات، ويتم تمثيل تبادل الأيونات **Ca2+-(Na+-K+)** ومنطقة تآكل الكربونات في مجال مثلث الكاتيونات. أظهر مخطط تشادا أن المياه المالحة كانت تتكون في الغالب من أيونات الصوديوم والكلوريد. توضح مخططات ستيف أن الصوديوم والبوتاسيوم والكالسيوم تهيمن على الكاتيونات، بينما تهيمن الكلورين على الأيونات مع وجود كمية أقل من البيكربونات. **LSI** و**RSI** و**PSI** و**AI** هي أمثلة لمؤشرات استقرار المياه التي تظهر إمكانية التكلس والتآكل.